Research Article

Fractional Analysis of MHD Boundary Layer Flow over a Stretching Sheet in Porous Medium: A New Stochastic Method

Imran Khan,[1] Hakeem Ullah [ID],[1] Hussain AlSalman [ID],[2] Mehreen Fiza,[1] Saeed Islam,[1] Muhammad Shoaib,[3] Muhammad Asif Zahoor Raja [ID],[4] Abdu Gumaei [ID],[5] and Farkhanda Ikhlaq[6]

[1]*Department of Mathematics, Abdul Wali Khan University Mardan, KP, Pakistan*
[2]*Department of Computer Science, College of Computer and Information Sciences, King Saud University, Riyadh, 11543, Saudi Arabia*
[3]*Department of Mathematics, COMSATS University Islamabad, Attock Campus, Attock 43600, Pakistan*
[4]*Future Technology Research Center, National Yunlin University of Science and Technology, 123 University Road, Section 3, Douliou, Yunlin 64002, Taiwan*
[5]*Computer Science Department, Faculty of Applied Sciences, Taiz University, Taiz 6803, Yemen*
[6]*Department of IT, Burraimi University College, Al Burraimi, Oman*

Correspondence should be addressed to Hakeem Ullah; hakeemullah1@gmail.com, Hussain AlSalman; halsalman@ksu.edu.sa, Muhammad Asif Zahoor Raja; rajamaz@yuntech.edu.tw, and Abdu Gumaei; abdugumaei@taiz.edu.ye

In this article, an effective computing approach is presented by exploiting the power of Levenberg-Marquardt scheme (LMS) in a backpropagation learning task of artificial neural network (ANN). It is proposed for solving the magnetohydrodynamics (MHD) fractional flow of boundary layer over a porous stretching sheet (MHDFF BLPSS) problem. A dataset obtained by the fractional optimal homotopy asymptotic (FOHA) method is created as a simulated data simple for training (TR), validation (VD), and testing (TS) the proposed approach. The experiments are conducted by computing the results of mean-square-error (MSE), regression analysis (RA), absolute error (AE), and histogram error (HE) measures on the created dataset of FOHA solution. During the learning task, the parameters of trained model are adjusted by the efficacy of ANN backpropagation with the LMS (ANN-BLMS) approach. The ANN-BLMS performance of the modeled problem is verified by attaining the best convergence and attractive numerical results of evaluation measures. The experimental results show that the approach is effective for finding a solution of MHDFF BLPSS problem.

1. Introduction

In many engineering and industrial processes, an incompressible flow liquid of boundary layer is common to be used over stretching sheet. This field has been paid attention by researchers in the last few decades. Boundary layer has wide ranges of applications in engineering industry. For instance, it is utilized in thermal wrapping, polymer paper aerodynamic extraction from debris, cooling plate without cooling tuber, glass-fiber development, and the boundary layer of liquid flow film in the phase of condensation [1–3]. Many metals require to be cool with continuous fibers through immersing them in quiescent liquids. The features of final mechanical product only depended on the temperature of the process and the drawing of the costs. Sakiadis [4, 5] investigated this area with the new work, and several researchers have explored the boundary flow layer into ongoing stretching sheet in increasing with increasing the speed. A solution of a closed form for viscous fluid flow that is incomprehensible than the advisory plate was discovered

by the author Crane [6]. Similarly, in [7], the authors studied the same magnetic flexible field wherein the fluid flow can absorb electrically a model or site of evaporation or injection, illustrated by the researcher Anderson [8]. In addition, Ariel [9] has examined the combination effect of the magnetic fields and the viscoelasticity on Crane's problem. Due to stretching sheet that occurs in different behaviors, the flow passing through it does not continuously require to be with two sizes. However, if the flow extension is radial, it could be with three. On the other hand, three stretches of flat surface with the same size of width were studied by author Wang [10]. In [11, 12], Brady and Acrivos monitored the flow that is inside the tube or channel and the flow that is performed outside the tube. Moreover, the authors in [13, 14] have evaluated the unstable property of the stretching sheet. In [15], the authors utilized homotopy perturbation method (HPM) and it is expanded for obtaining a solution in axisymmetric analysis of the flow in a flat layer. Samuel and Hall [16] provided noniterative solutions to the MHD flow. Magnetohydrodynamics (MHD) concerns with studying the interaction of electromagnetic conditions and the transfer of liquid heat. The flow of conducting fluids is essential in many areas and fields of engineering and science, such as MHD pumps, MHD power generation, and MHD generators. Recently, many researchers worked on BL flow [17–25]. These studies are done by analytical/numerical approach. The recent usage of stochastic numerical computing solvers are thermodynamics, offline circuits, astrophysics, atomic physics, plasma physics, MHD, dynamics of fluid, bioinformatics, nanotechnology, electromagnetics, electricity, theories of random matrix, energy, and finance [26–41]. In addition, to solve different statistics [42, 43], stochastic computing solutions are used.

The mechanisms of proposed stochastic are as follows:

(i) An effective application of artificial intelligence-based computing is introduced by means of artificial neural network backpropagation with the Levenberg-Marquardt scheme (ANN-BLMS) for achieving a solution to MHDFF BLPSS at different scenarios on variation of Deborah, porosity, and magnetic numbers

(ii) The mathematical modeling of the work is formulated with nonlinear coupled PDEs to MHDFF BLPSS. The PDEs are converted to their equivalent nonlinear ODE structure using the similarity of variables

(iii) A dataset is created to evaluate the proposed ANN-BLMS at several variations of MHDFF BLPSS on the basis of Deborah, porosity, and magnetic parameters

(iv) The phases of training, validation, and testing for the ANN-BLMS are given by demonstrating the MHDFF BLPSS at a set of scenarios and comparisons with the reference numerical results to validate the applicability and effectiveness of the proposed ANN-BLMS
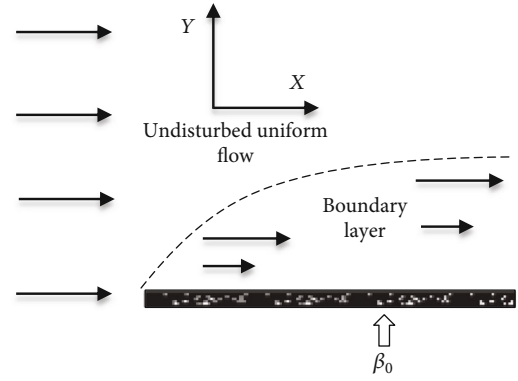

Figure 1: Sketch of the flow problem.

(v) The performance results of ANN-BLMS for solving the MHDFF BLPSS is further confirmed by the convergence plots of the mean squared errors, fitting graphs, histogram errors, and regression analysis curves

2. Problem Formulation

We consider an incompressible viscous flow over a flat porous plate. The fluid is electrically conducting under the influence of applied magnetic field $\beta(x)$ normal to the stretching sheet as shown in Figure 1.

The fundamental equations [44] are as follows:

$$\nabla \cdot W = 0, \tag{1}$$

$$\frac{\partial W}{\partial u} + (W \cdot \nabla) W = \frac{1}{\rho} \nabla p + \mu \nabla^2 W - \frac{1}{\rho} (J \times \beta) W - \frac{\mu}{\rho k} W, \tag{2}$$

where $W = (x(u, v), y(u, v), 0)$, β is the magnetic field, and J is the current density.

The boundary conditions (BCs) are used.

$$\begin{aligned} x(i, 0) &= ci^n, \\ y(i, 0) &= 0, \\ u(i, \infty) &= 0. \end{aligned} \tag{3}$$

This model is generalized through changing the first time derivative by the fractional derivative with order α, $1 < \alpha < 2$. The fractional time model of Navier–Stokes equation then takes the following form:

$$D_u^\alpha W + (W \cdot \nabla) W = -\frac{1}{\rho} \nabla p + y \nabla^2 W - \frac{1}{\rho} (J \times \beta) W - \frac{\mu}{\rho k} W, \tag{4}$$

where D_u^α is the Caputo fractional derivative of order α.

For reducing the governing equation of the boundary value problem, the similarity transformation is performed using the following equations [44]:
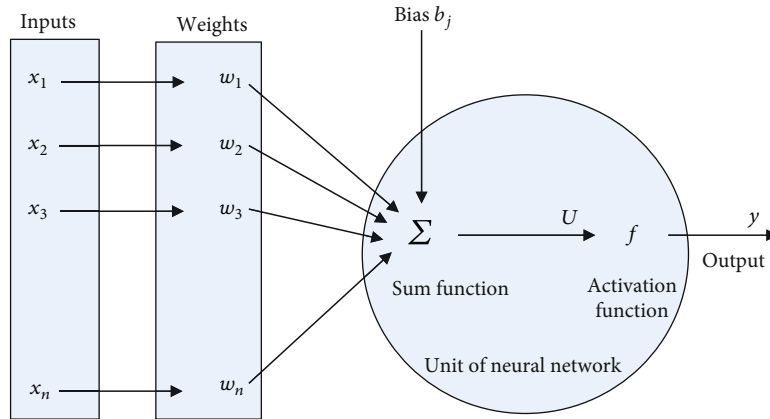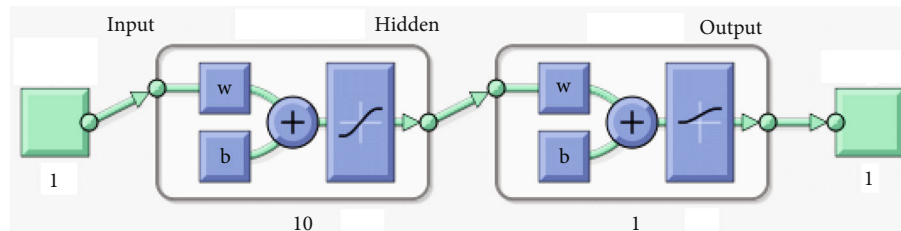
FIGURE 2: A single neural network structure.

FIGURE 3: A general representation of ANN-BLMS input, output, and hidden layer.

$$x(i, v) = xi^{v} f'(\eta),$$

$$\eta = v \sqrt{\frac{c(r+1)}{2y}} i^{(r-1)/2} v, \tag{5}$$

$$y(\eta) = -\sqrt{\frac{c(r+1)}{2}} i^{(r-1)/2} \left[f(\eta) + \frac{(r-1)}{(r+1)} \eta f'(\eta) \right].$$

We obtain

$$D_u^\alpha W + \frac{\partial^3 f}{\partial \eta^3} + f \frac{\partial^2 f}{\partial \eta^2} - \beta \left(\frac{\partial f}{\partial \eta} \right)^2 - M \frac{\partial f}{\partial \eta} - \gamma \frac{\partial f}{\partial \eta} = 0,$$

$$f(0) = 0,$$

$$\frac{\partial f}{\partial \eta}(0) = 1, \tag{6}$$

$$\frac{\partial f}{\partial \eta}(\infty) = 0,$$

where $\beta = 2n/(1+n)$, $\gamma = \mu/(\rho r(1+n))$, $M = 2\sigma \beta_0^2/(\rho c(1+n))$.

Definition 1. The Riemann-Liouville fractional integral operator [45].

$$J^\alpha f(\eta) = \frac{1}{\Gamma(\alpha)} \int_0^u (u - \tau)^{m-1} f(\tau) d\tau,$$

$$J^\alpha f(\eta) = f(\eta), \tag{7}$$

$$J^\alpha u^\xi = \frac{\Gamma(\xi + \alpha)}{\Gamma(\xi + \alpha + 1)} u^{\alpha + m}.$$

Definition 2. The fractional derivative of the function, $f(u)$, in the Caputo sense [46].

$$D_u^\alpha f(u) = \frac{1}{\Gamma(m - \alpha)} \int_0^u (u - \tau)^{m-\alpha-1} f^m(\tau) d\tau. \tag{8}$$

Definition 3. The Laplace of Caputo [46].

$$L[D_u^\alpha f(u)] = s^\alpha L[f(u)] - \sum_{r=0}^{n-1} s^{\alpha-n-1} f^\tau(\tau). \tag{9}$$

3. Solution Procedure of the New Stochastic Method

Figure 2 shows the single neural network structure of the proposed ANN-BLMS model. The design of our ANN-BLMS model contains ten neurons, as visualized in Figure 3. Also, the general procedure of ANN-BLMS is presented step by step and specified by Figure 4. ANN-BLMS is accomplished with the help of nftool in MATLAB by setting the parameters to fit the neural network model with the
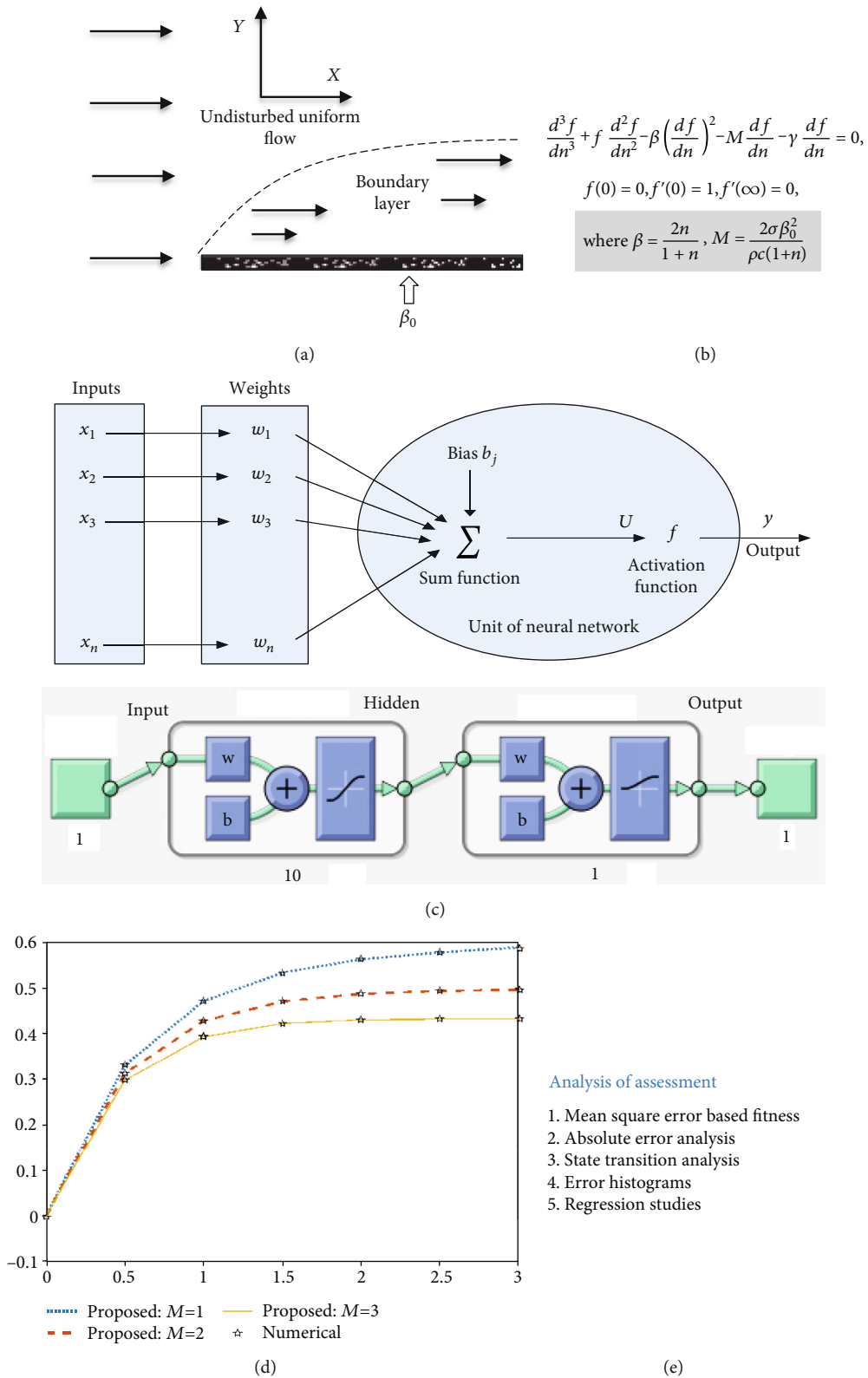
$$\frac{d^3f}{dn^3} + f\frac{d^2f}{dn^2} - \beta\left(\frac{df}{dn}\right)^2 - M\frac{df}{dn} - \gamma\frac{df}{dn} = 0,$$

$$f(0) = 0, f'(0) = 1, f'(\infty) = 0,$$

$$\text{where } \beta = \frac{2n}{1+n}, M = \frac{2\sigma\beta_0^2}{\rho c(1+n)}$$

(a)

(b)

(c)

Analysis of assessment

1. Mean square error based fitness
2. Absolute error analysis
3. State transition analysis
4. Error histograms
5. Regression studies

(d)

(e)

Figure 4: The methodology workflow of ANN-BLMS for MHDFF BLPSS: (a) sketch of the flow problem, (b) problem formulation, (c) developed intelligent computing network model, (d) results, and (e) comparative analysis.

functioning of Levenberg-Marquardt backpropagation and updating the neural network model's weights. It is clear from analysis that the ANN-BLMS is implemented for the fluidic model MHDFF BLPSS. Set the values of one parameter β and treating the other physical parameters γ, M as fixed. In the same fashion, the other parameters are changeable and there are a total of three scenarios with three cases for every scenario as exposed in Table 1. For using the ANN-BLMS, we used the step size 0.03 between the intervals of the problem by using the FOHA method. Selecting randomly 80%, 10%, and 10% for the testing, training, and validation from 201 data input points of f values is employed for conducting the experiments. The TR dataset is exploited for training the model, and VD is utilized for validating of the trained model, while the TS dataset is used to test the model and get the performance results for evaluation.

The single-layer structure of neural networks (input, hidden, and output layers) is displayed in Figure 4.

4. Analysis of Results

The proposed ANN-BLMS is evaluated on three scenarios, and each scenario has three cases, as given in Table 1. Figures 5–6 show the state transition's results and the other performance results, as well as the fitting plots of the proposed solution are given through Figures 7–12. In Figure 13, we can see the plots of HEs, and from Figures 14–19, we can see the regression analysis results of the MHDFF BLPSS. For cases 1 and 3 of all scenarios, the MSEs of TR, VLD, and TS datasets are exposed in Figures 5(a)–5(f). From Figures 5(a)–5(f), we can notice that best performance result has been attained at epochs [1000, 324, 366, 143, 73, 24] with MSEs of about [1.3224×10^{-10}, 4.702×10^{-9}, 1.21138×10^{-8}, 5.02766×10^{-7}, 2.7001×10^{-5}, and 1.0658×10^{-9}], correspondingly.

The best performance is established for every scenario in which suitable values of the step size (Mu) for the gradient descent (GD) and Levenberg-Marquardt are [$1.0553 \times 10 - 07$, $9.9298 \times 10 - 08, 9.9259 \times 10 - 08$, $8.4492 \times 10 - 7$, $9.7359 \times 10 - 8$, and $9.6455 \times 10 - 8$] and [10-08, 10-8, 10-08, 10-08, 10-09], as presented in Figures 6(a)–6(f). From these figures and results, it is clearly demonstrated that the ANN-BLMS is accurate and a reliable convergence in every case of MHDFF BLPSS. For cases 1 and 3 of all scenarios of MHDFF BLPSS model, the effectiveness of ANN-BLMS is scrutinized with the reference numerical results of OHAM along with the errors of dynamics shown in Figures 7–12. We see that the maximum errors achieved on the VL and TS of the ANN-BLMS model are less than [$0.3 \times 10 - 03$, $0.1 \times 10 - 03$, $0.1 \times 10 - 3, 3 \times 10 - 03$, $0.5 \times 10 - 03$, and $0.9 \times 10 - 05$], as illustrated in Figures 7–12. The errors' variability is similarly measured with HE results, which are specified in Figures 13(a)–13(f). Also, we can see that the maximum errors attained with reference results and a value of errors are less than [-2.37 E-7, -3.5E-6, 3.64E-4, -1.2E-4, -1.1E-4, and -2.5E-5] in all the cases of the MHDFF BLPSS.

The investigation concluded by regression analysis is accompanied using co-relation readings. The results of regression analysis are clarified by Figures 14–19. The study

Table 1: A description of adopted scenarios and cases to boundary layer flow model with physical parameters of interest.

Scenario number	Case number	Physical quantity		
		β	γ	M
1	1	1	1	1
	2	2	1	1
	3	3	1	1
2	1	1	1	1
	2	1	2	1
	3	1	3	1
3	1	1	1	1
	2	1	1	2
	3	1	1	3

of co-relation is piloted by regression studies. The results of regression for each scenario are around unity values of the co-relation (R) and are reliable, which means that testing training and validations are accurately modeled to perform the ANN-BLMS. Moreover, for all three cases of each scenario of MHDFF BLPSS, the convergence attains good outcomes in terms of MSEs, regression analysis, and other backpropagation performance measures, as demonstrated by Table 2 for all cases of every scenario, separately.

The performance results are about 10-04 to 10-07, 10-8 to 10-10, and 10-06 to 10-08 for all the scenarios with cases 1 and 3 of MHDFF BLPSS. These results demonstrate that the performance of ANN-BLMS is stable for every case of model for the MHDFF BLPSS. The effects of the physical parameters on the velocity profile based on the results of ANN-BLMS are given by Figures 20(a), 21(a), and 22(a). The variation (rise) of the physical parameter Deborah number β results to a decrease in the velocity value of the profile. Initially, the effect of β is very small in interval [0,0.5] and the effect of increasing β is very clear in 0.5 to 3, which caused the decrease in the velocity profile, as shown in Figure 20(a). Similarly, the effects of porosity and magnetic parameters γ and M on velocity profile are obtained in Figures 21(a) and 22(a), respectively. It is observed that by the increase in the values of γ, M, a decreasing in velocity value of profile (boundary layer thickness) is observed. These parameters have low effects near the origin and have a clear impact away from the origin.

By increasing values of physical parameters γ, β, and M, decreasing in the velocity profiles is detected. It is because of the fact that the parameters that increase the opposing forces can turn to reduce the velocity value of the profile. The ANN-BLMS results are verified by comparing them with the numerical reference results, and hence, the validation of our method is proved. In Figures 20(b), 21(b), and 22(b), the absolute errors (AEs) are shown for all scenarios. It is obvious to show that the AEs are observed with 10-03 to 10-05, 10-02 to 10-08, and 10-04 to 10-07, respectively. These explanations obviously indicate the performance of ANN-BLMS for solving the fluid application. Still, the AEs validate the accuracy and precision of the method.
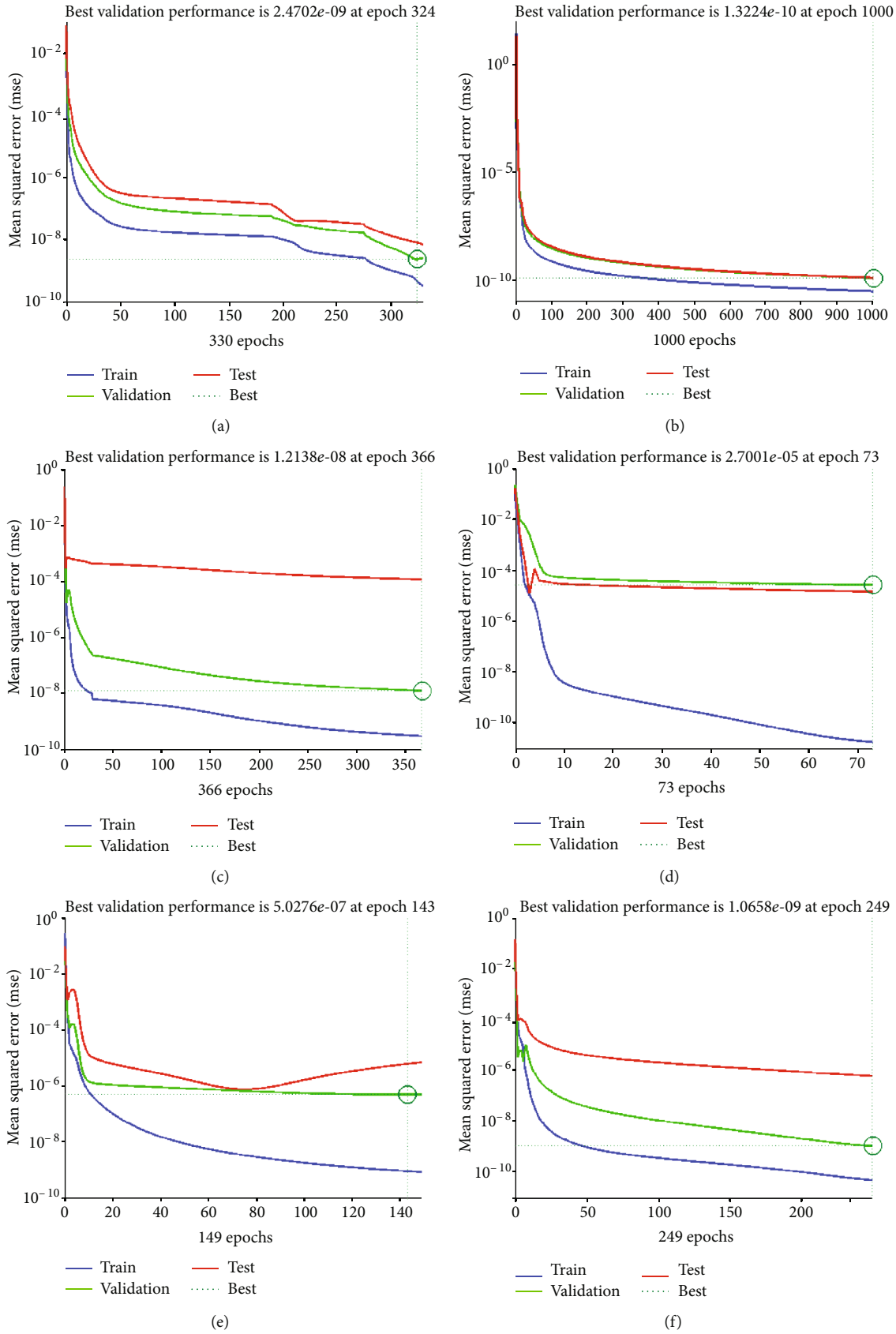
FIGURE 5: Performance of MSEs for the proposed ANN-BLMS to solve MHDFF BLPSS: (a) MSE result of case 1 in scenario 1, (b) MSE result of case 3 in scenario 1, (c) MSE result of case 1 in scenario 2, (d) MSE result of case 3 in scenario 2, (e) MSE result of case 1 in scenario 3, and (f) MSE result of case 3 in scenario 3.
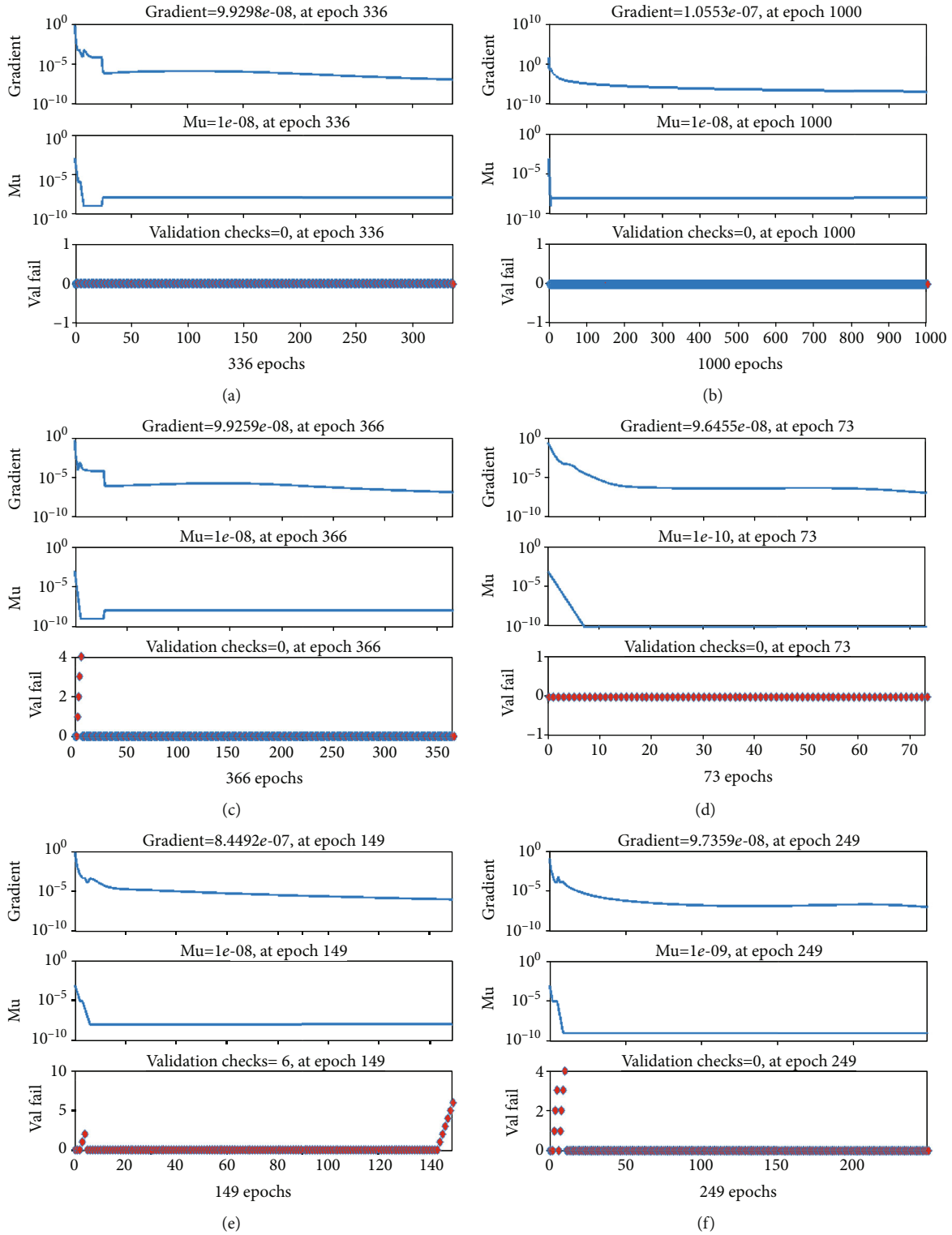
FIGURE 6: State transitions of the proposed ANN-BLMS for solving MHDFF BLPSS: (a) state transition result of case 1 in scenario 1, (b) state transition result of case 3 in scenario 1, (c) state transition result of case 1 in scenario 2, (d) state transition result of case 3 in scenario 2, (e) state transition result of case 1 in scenario 3, and (f) R state transition result of case 3 of scenario 3.
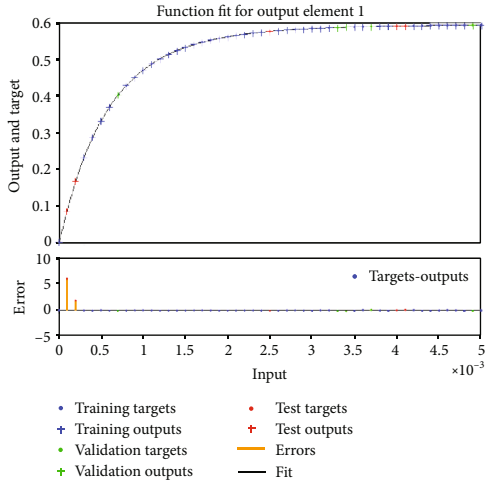
FIGURE 7: The results of ANN-BLMS compared to reference numerical results of case 1 for scenario 1 of MHDFF BLPSS.

FIGURE 8: The results of ANN-BLMS compared to reference numerical results of case 3 for scenario 1 of MHDFF BLPSS.
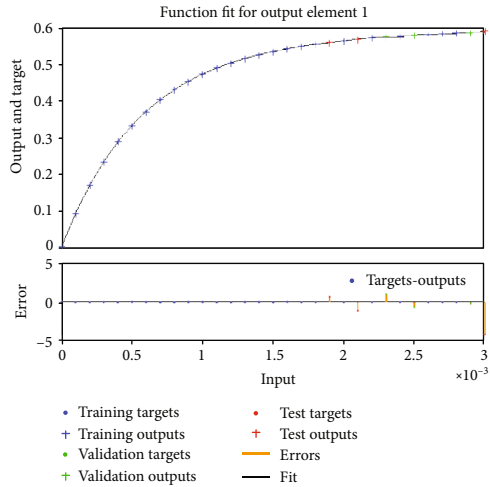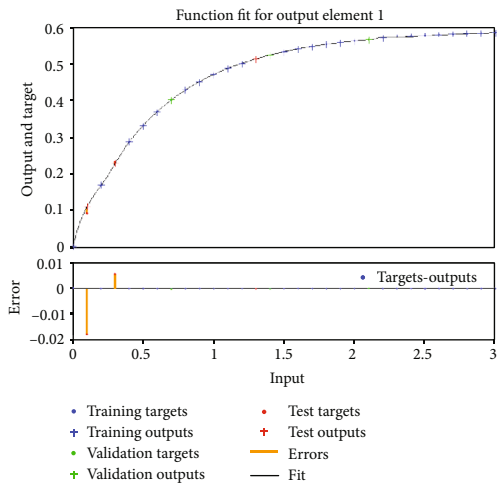

FIGURE 9: The results of ANN-BLMS compared to reference numerical results of case 1 for scenario 2 of MHDFF BLPSS.
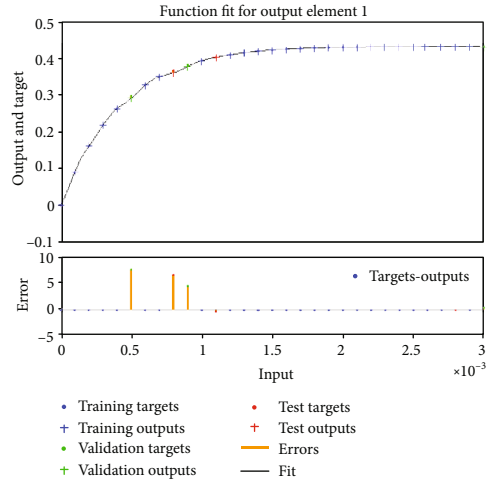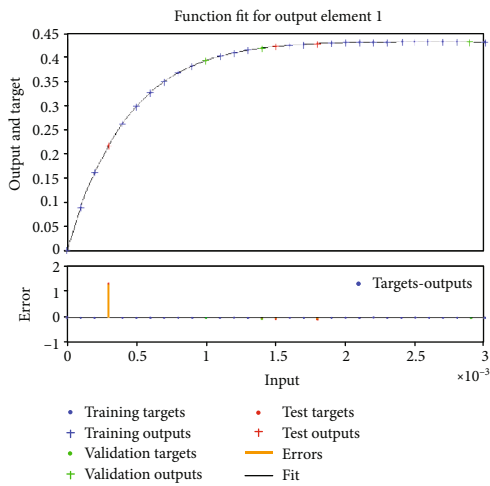

FIGURE 10: The results of ANN-BLMS compared to reference numerical results of case 3 for scenario 2 of MHDFF BLPSS.

FIGURE 11: The results of ANN-BLMS compared to reference numerical results of case 1 for scenario 3 of MHDFF BLPSS.

FIGURE 12: The results of ANN-BLMS compared to reference numerical results of case 3 for scenario 3 of MHDFF BLPSS.
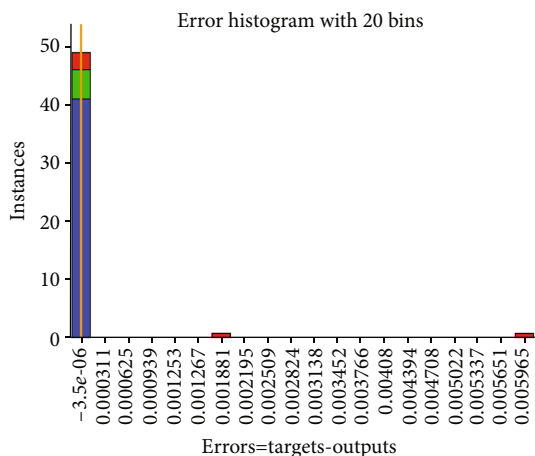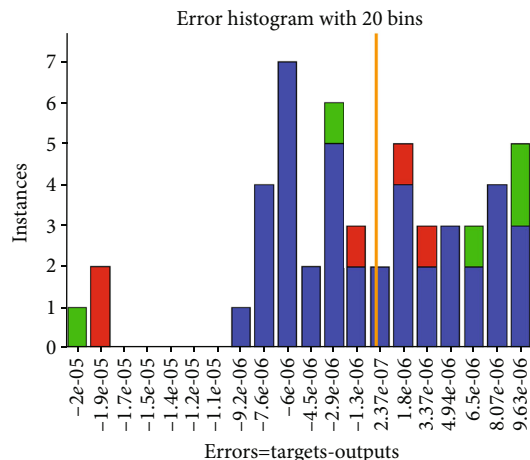
Error histogram with 20 bins
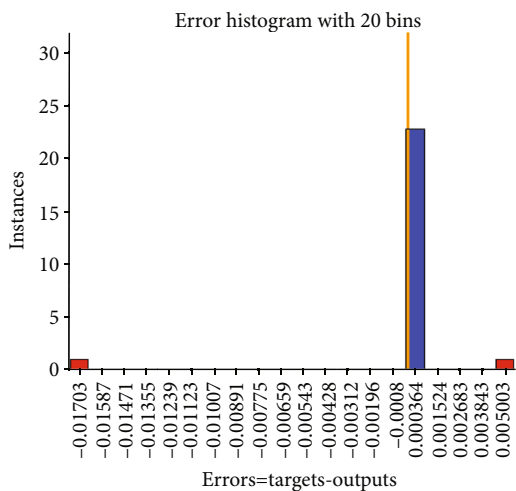

(a)

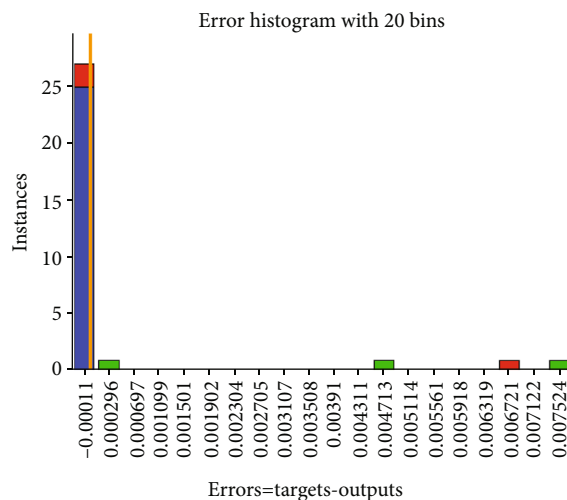Error histogram with 20 bins

(b)

Error histogram with 20 bins

(c)

Error histogram with 20 bins
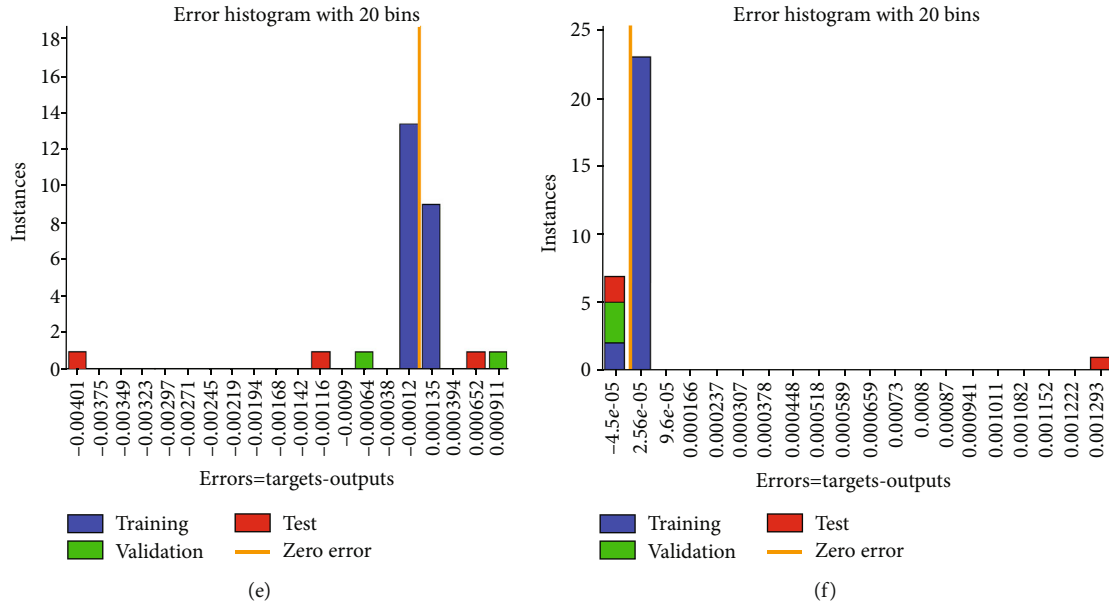

(d)

FIGURE 13: Continued.

FIGURE 13: Histogram errors (HEs) for the proposed ANN-BLMS in cases 1 and 3 of all scenarios to solve MHDFF BLPSS: (a) histogram errors of case 1 in scenario 1, (b) histogram errors of case 3 in scenario 1, (c) histogram errors of case 1 in scenario 2, (d) histogram errors of case 3 in scenario 2, (e) histogram errors of case 1 in scenario 3, and (f) histogram errors of case 3 in scenario 3.

FIGURE 14: Regression analysis graph of the ANN-BLMS approach for case 1 in scenario 1 of MHDFF BLPSS.

FIGURE 15: Regression analysis graph of the ANN-BLMS approach for case 3 in scenario 1 of MHDFF BLPSS.

Figure 16: Regression analysis graph of the ANN-BLMS approach for case 1 in scenario 2 of MHDFF BLPSS.

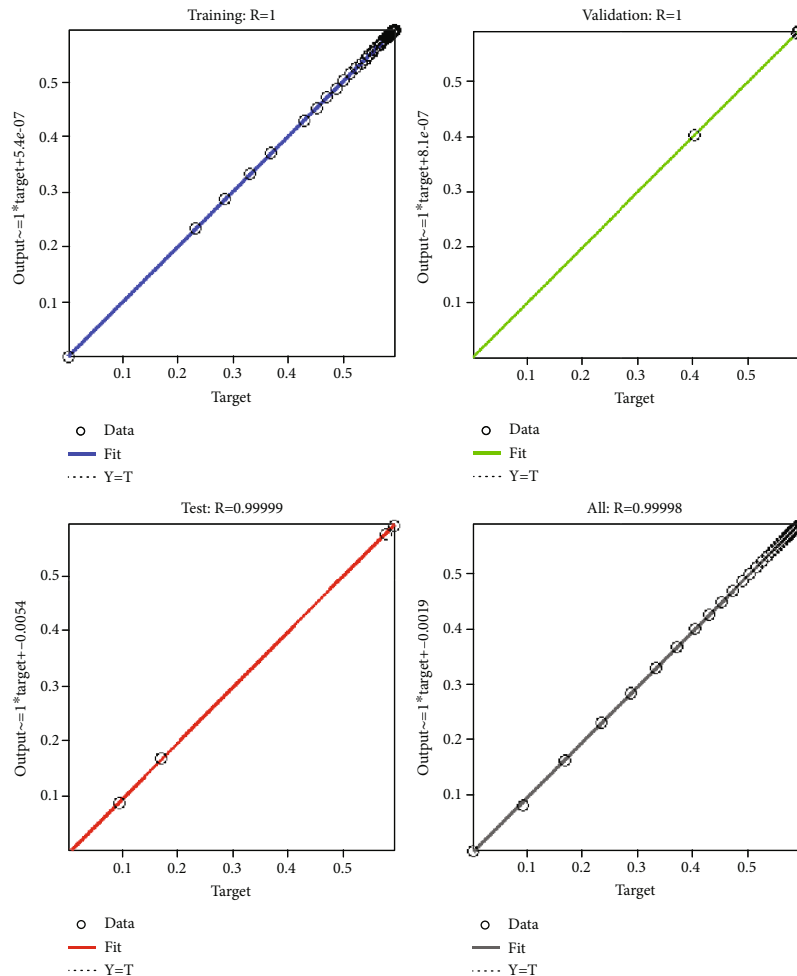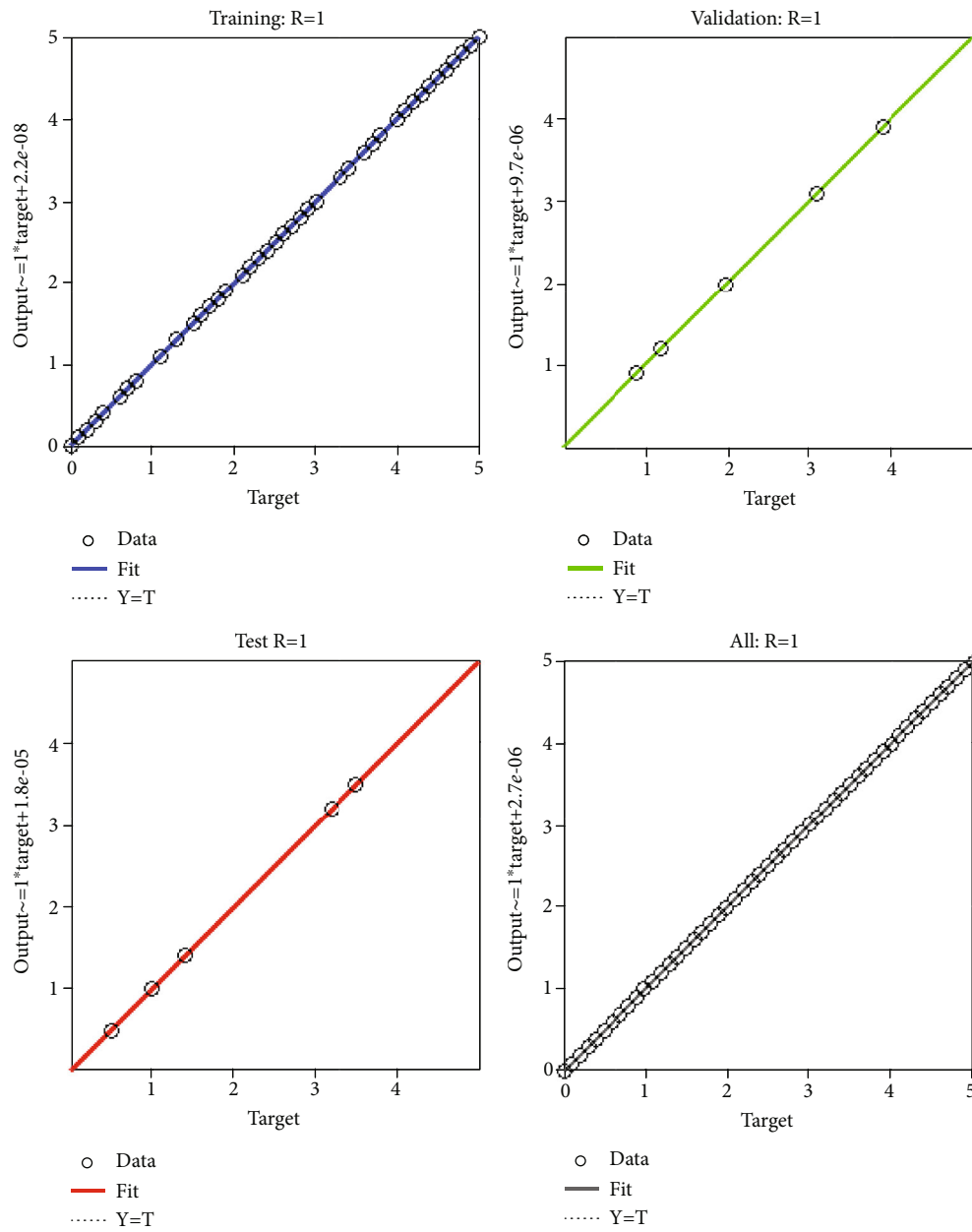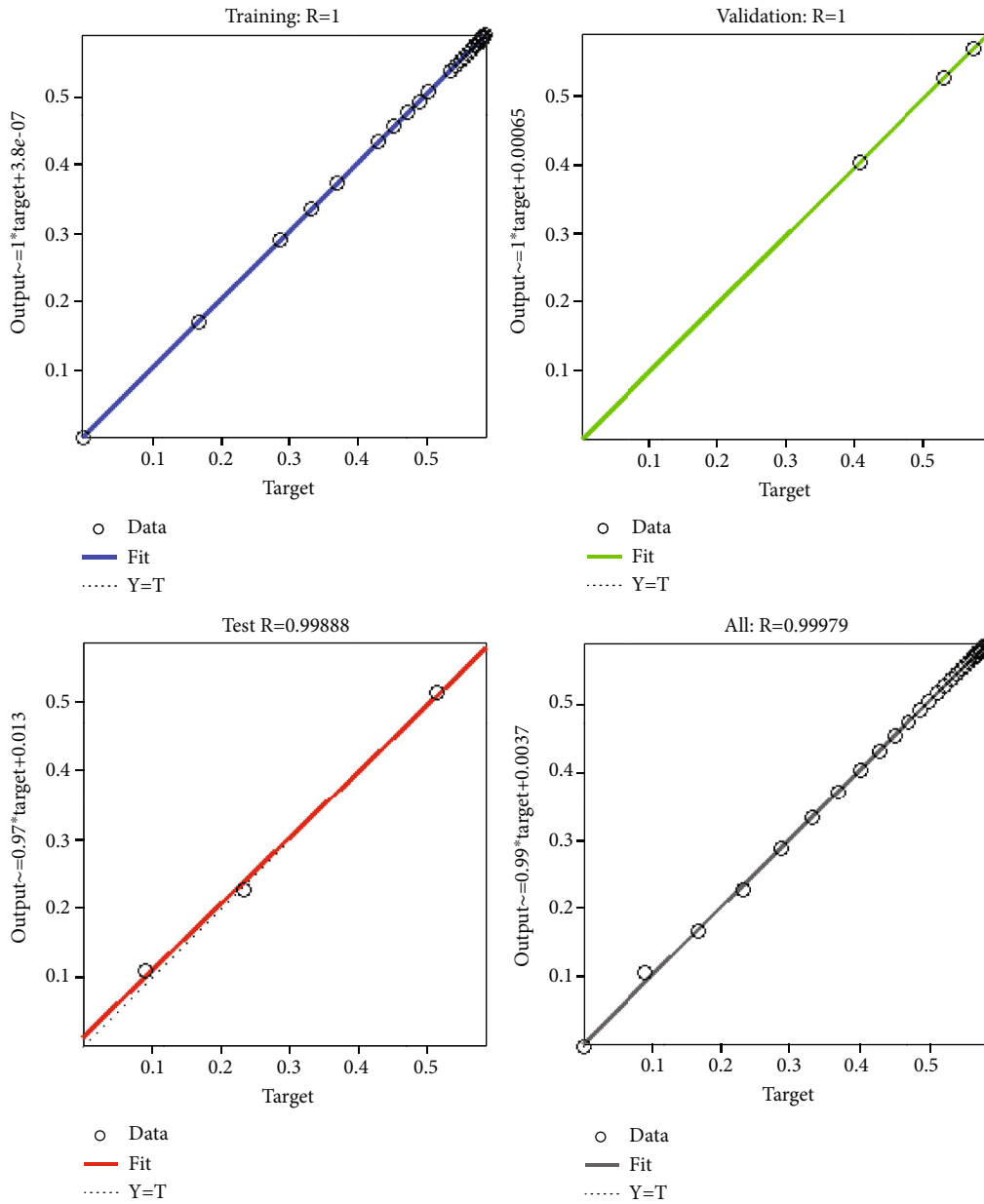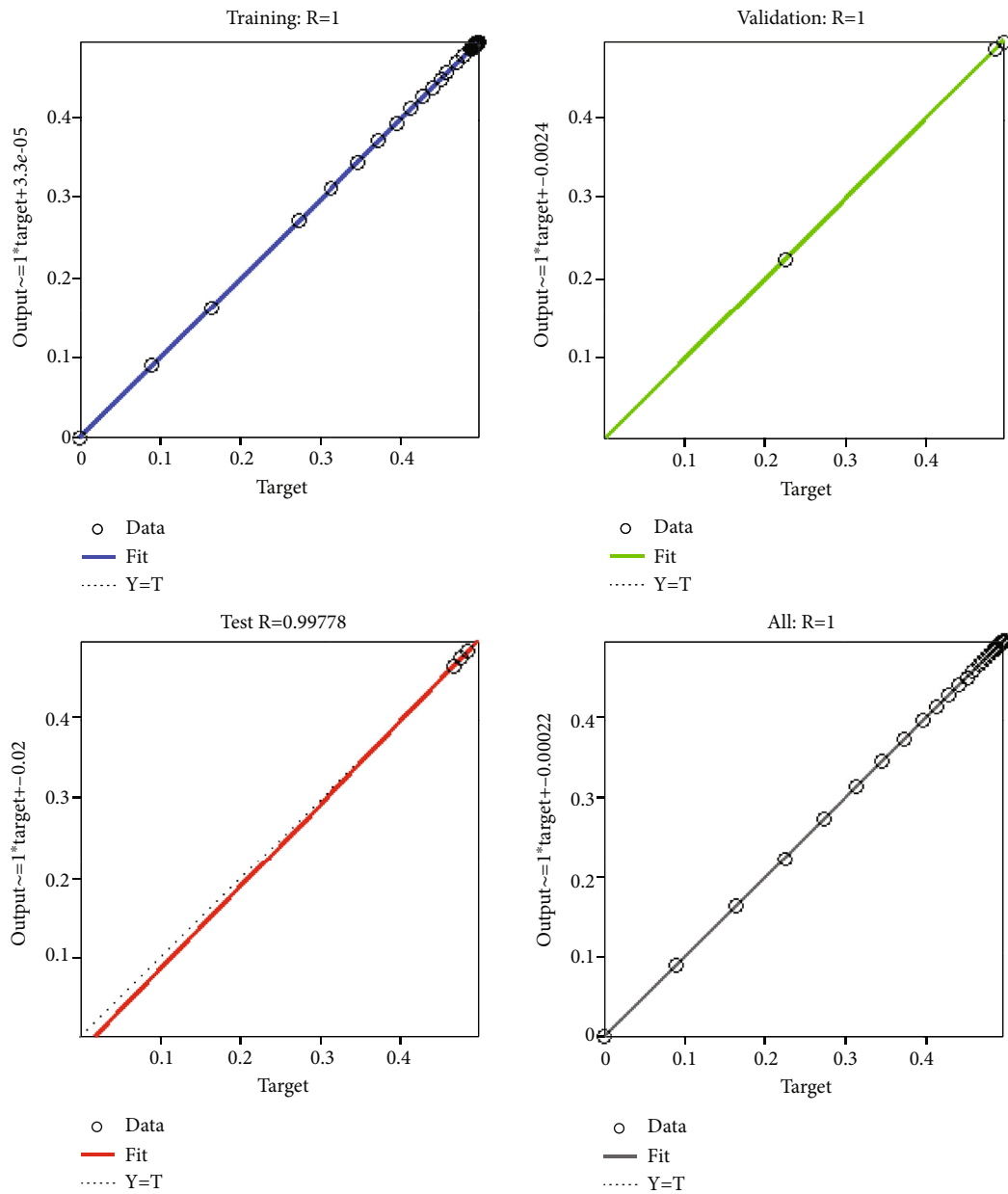FIGURE 17: Regression analysis graph of the ANN-BLMS approach for case 3 in scenario 2 of MHDFF BLPSS.
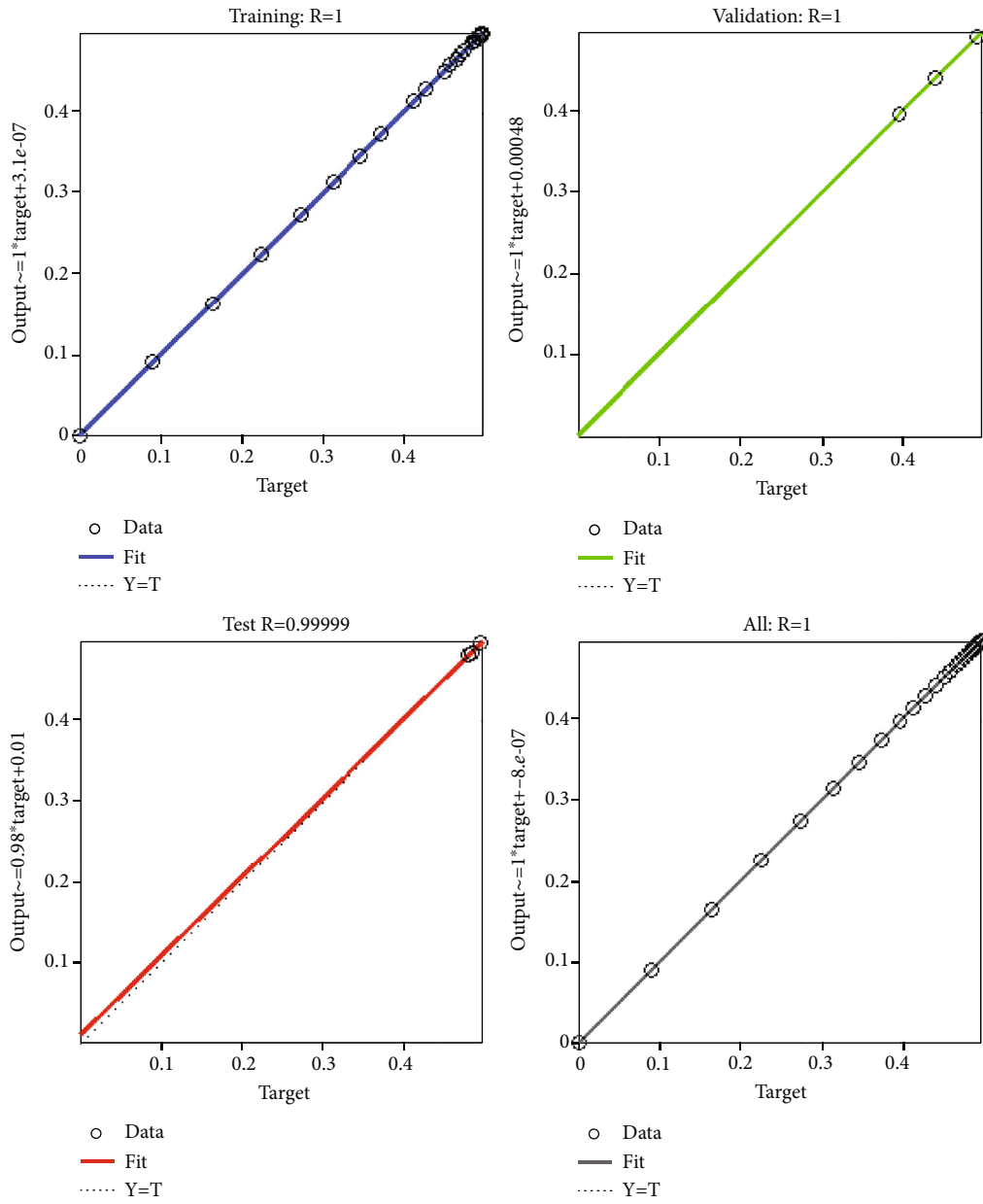
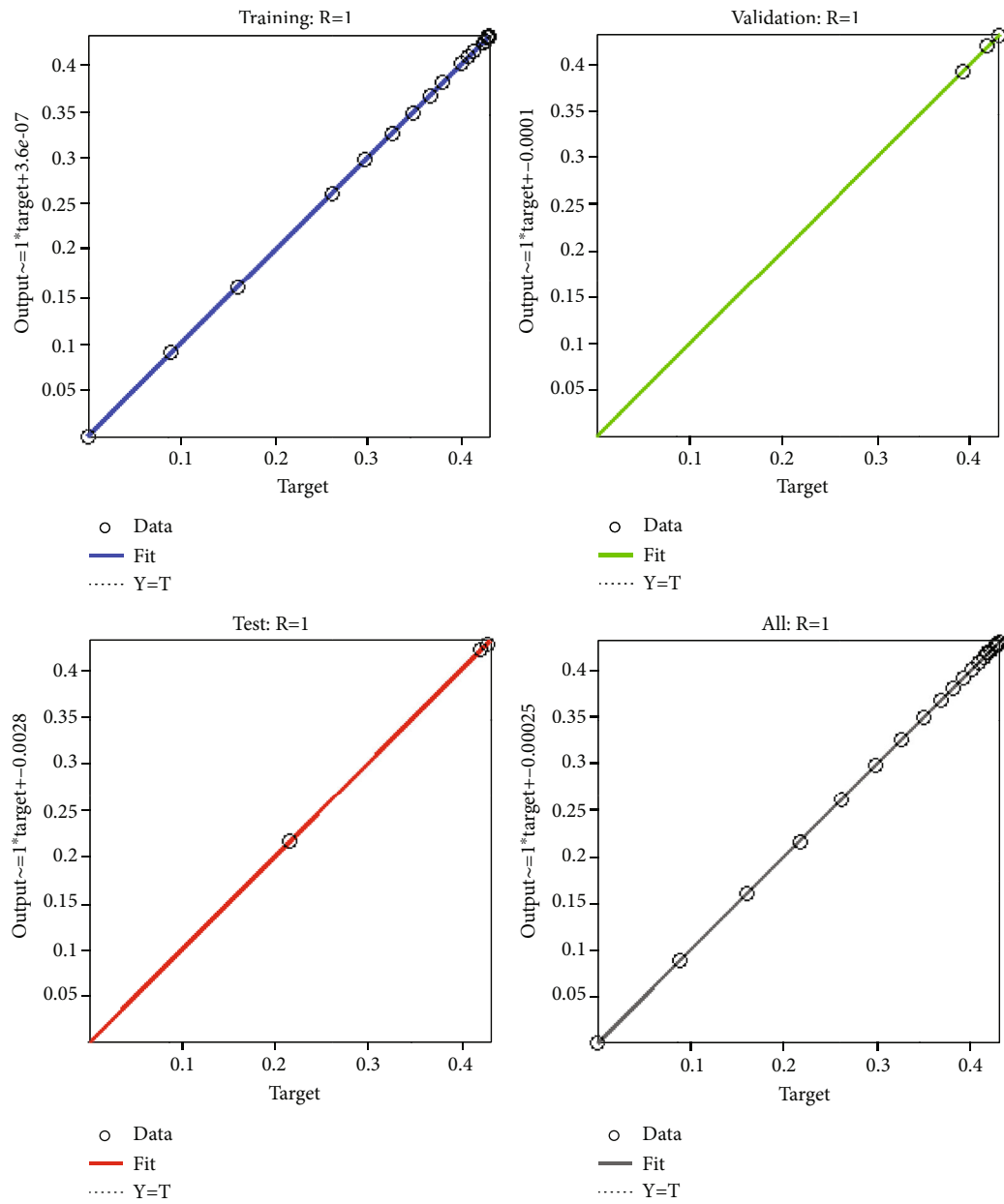FIGURE 18: Regression analysis graph of the ANN-BLMS approach for case 1 in scenario 3 of MHDFF BLPSS.

FIGURE 19: Regression analysis graph of the ANN-BLMS approach for case 3 in scenario 3 of MHDFF BLPSS.

TABLE 2: Experimental results of ANN-BLMS for all cases of scenarios 1, 2, and 3 of MHDFF BLPSS.

No. of	Mean square errors			Performance	Gradients	Mu	Epochs	Time
Scenario 1 cases								
1	9.665419E-10	1.015905E-8	8.26437E-6	9.67E-10	9.93E-08	1.00E-08	336	<1
2	1.744190E-5	8.33558E-8	2.6077E-6	3.33E-11	1.06E-07	1.00E-08	11	<1
3	3.33326E-11	1.32238E-10	1.35543E-10	3.33E-11	1.06E-07	1.00E-08	1000	<1
Scenario 2 cases								
1	3.0384E-10	1.2138E-08	1.1378E-04	3.04E-10	9.93E-08	1.00E-08	366	<1
2	9.3526E-10	6.3979E-07	3.8721E-07	7.59E-10	1.28E-07	1.00E-8	70	<1
3	1.9107E-11	2.7001E-05	1.501E-07	7.59E-11	9.65E-08	1.00E-8	73	<1
Scenario 3 cases								
1	9.31098E-10	5.02758E-07	6.25522E-06	8.65E-10	8.45E-07	1.00E-08	149	<1
2	1.58051E-10	4.36870E-09	2.41002E-08	1.58E-10	9.98E-08	1.00E-08	603	<1
3	4.91107E-11	1.06570E-09	5.91223E-07	4.91E-11	9.74E-08	1.00E-08	249	<1

(a)

(b)

FIGURE 20: Comparisons for the ANN-BLMS results and the reference results regarding scenario 1 of MHDFF BLPSS: (a) variation of performance at different values of β and (b) absolute error (AE) analysis.

(a)

(b)

FIGURE 21: Comparisons for the ANN-BLMS results and the reference results regarding scenario 2 of MHDFF BLPSS: (a) variation of performance at different values of γ and (b) absolute error (AE) analysis.
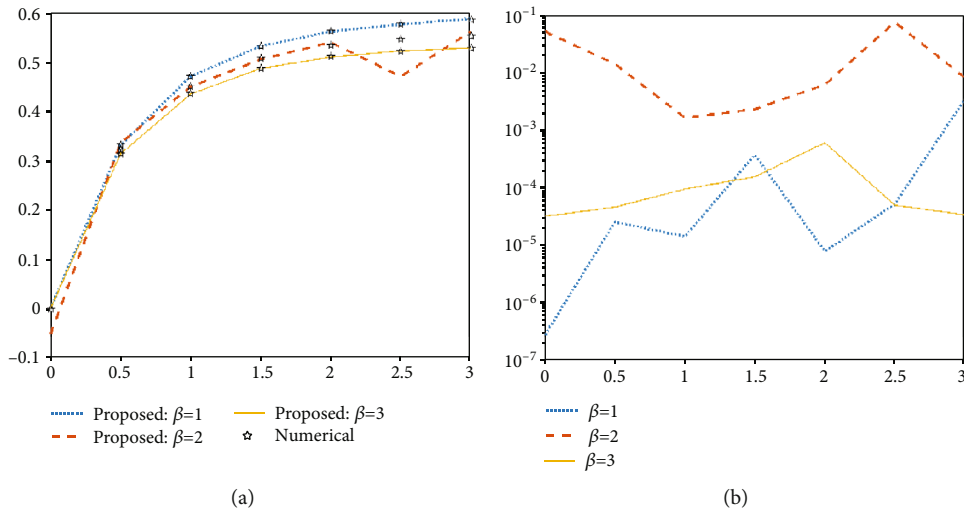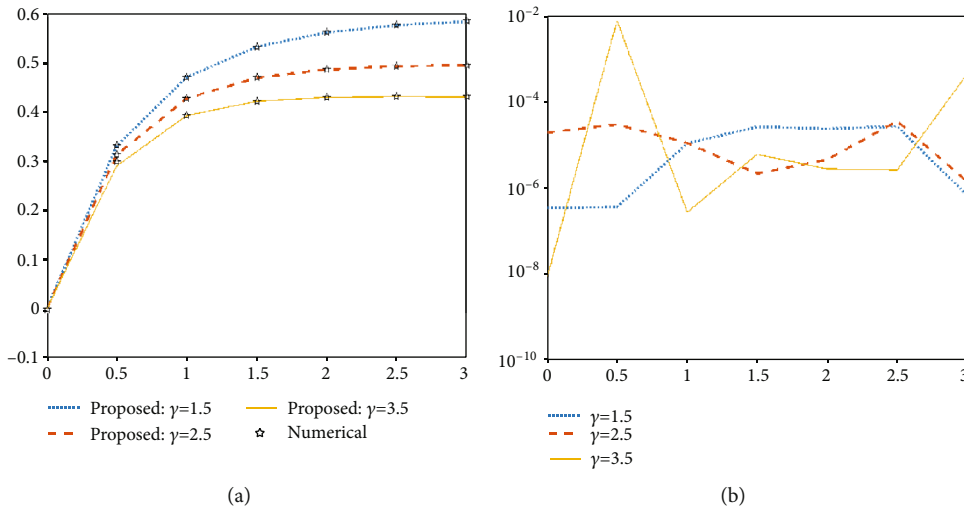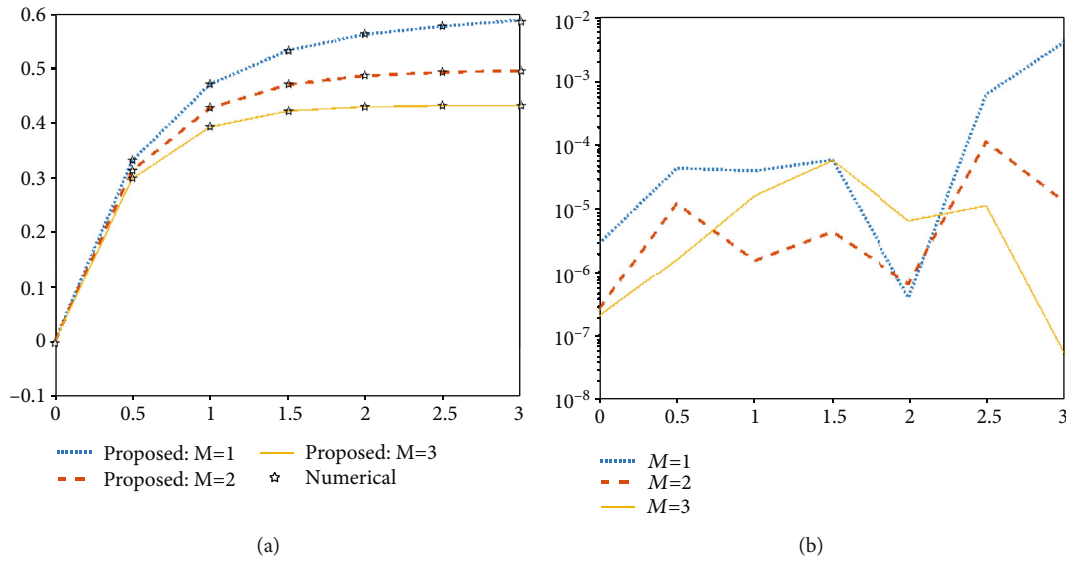
(a)

(b)

FIGURE 22: Comparisons for the ANN-BLMS results and the reference results regarding scenario 3 of MHDFF BLPSS: (a) variation of performance at different values of M and (b) absolute error (AE) analysis.
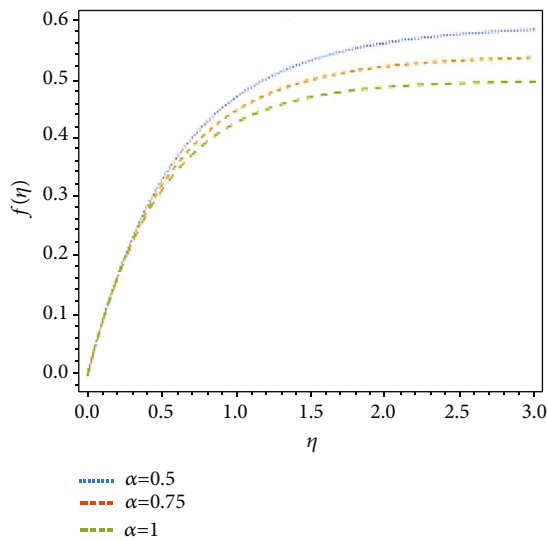

FIGURE 23: Variations of fractional order.

Furthermore, Figure 23 demonstrates the variations of fractional derivative at different values of order α. It shows that the ANN-BLMS model can be generalized through changing the fractional derivative at order values $\alpha = 0.5$, $\alpha = 0.75$, and $\alpha = 1$. Therefore, we can conclude that the fractional order of the model with changed orders can give a better fitting with fluid actual data.

5. Conclusion

In this paper, an effective computing approach is proposed by exploiting the power of Levenberg-Marquardt scheme (LMS) for backpropagation learning task. It is applied for solving the magnetohydrodynamics (MHD) fractional flow of boundary layer over a porous stretching sheet (MHDFF BLPSS) problem. A simulated dataset is generated by the fractional optimal homotopy asymptotic (FOHA) method for training (TR), validation (VD), and testing (TS) the proposed approach. The main strength of the ANN-BLMS approach is exploited for a numerical solution to MHDFF BLPSS after performing the PDE transformation. This transformation is based on the flow of the model into an ODEs system using the conversion of the similarity variables. The optimal homotopy asymptotic method is utilized for generating the dataset of the flow model. The ratio of training, testing, and validation from the dataset of ANN-BLMS at different scenarios is specified by 80%, 10%, and 10%, respectively. The comparison between both the results of proposed model and the reference numerical results is employed for evaluation. The experimental results and comparisons showed that the developed model gives better accurate outputs and results for the fluidic system in its required considerations. Therefore, the performance and efficacy of ANN-BLMT approach for solving the flow model appear through mean squared errors (MSEs), regression analysis metric, performance measure, and histogram errors (HEs), and absolute errors (AEs). Some of the key points are given as follows:

(i) ANN-BLMS takes a less computational cost, as well as it has fast convergent and does not require linearization

(ii) ANN-BLMS is simple in applicability

(iii) ANN-BLMS has a good performance compared with other numerical approaches and methods

(iv) ANN-BLMS can minimize the results of absolute error measure

(v) The effectiveness of ANN-BLMS is assessed by measuring the MSEs, HEs, RA, AEs, and FT metrics on 80% training, 10% test, and 10% validation data samples

(vi) Also, the physical variation of the approach parameters indicates that the boundary layer thickness decreases by the increase in the values of Deborah, porosity, and magnetic parameters

(vii) The boundary layer flows have many applications in engineering and industries such as "hot rolling, aerodynamic extrusion of a polymer sheet from a die, boundary layer along a liquid film in condensation process, cooling of an infinite metallic plate in a cooling bath, and glass–fiber production"

(viii) The conducting boundary layer flows have industrial and engineering applications like MHD generators, MHD power generation, and MHD pump productions

(ix) This procedure will be used for the nanofluid flow problems and nanotechnology

In future work, the new platforms and applications using artificial intelligence methods will be implemented for solving flow issues in a more effective way. Moreover, we plan to apply this method to recent developments in nanotechnology, energy, biological models, and detecting spreading diseases like COVID-19.

Data Availability

The data used in this study are hypothetical and can be used by anyone by just citing this article.

Conflicts of Interest

The authors declare no conflicts of interest.

Acknowledgments

References

[1] T. Alten, S. Oh, and H. Gegrl, *Metal Forming Fundamentals and Applications*, American Society of Metals, Metal Park, 1979.

[2] E. G. Fisher, *Extrusion of Plastics*, Wiley, New York, 1976.

[3] Z. Tadmor and I. Klein, *Engineering Principles of Plasticating Extrusion, Polymer Science and Engineering Series*, Van Nostrand Reinhold, New York, 1970.

[4] B. C. Sakiadis, "Boundary-layer behavior on continuous solid surfaces: I. Boundary-layer equations for two-dimensional and axisymmetric flow," *AICHE Journal*, vol. 7, no. 1, pp. 26–28, 1961.

[5] B. C. Sakiadis, "Boundary-layer behavior on continuous solid surfaces: II. The boundary layer on a continuous flat surface," *AICHE Journal*, vol. 7, no. 2, pp. 221–225, 1961.

[6] L. J. Crane, "Flow past a stretching plate," *Zeitschrift für Angewandte Mathematik und Mechanik*, vol. 21, no. 4, pp. 645–647, 1970.

[7] P. S. Gupta and A. S. Gupta, "Heat and mass transfer on a stretching sheet with suction or blowing," *Canadian Journal of Chemical Engineering*, vol. 55, no. 6, pp. 744–746, 1977.

[8] H. I. Anderson, "MHD flow of a viscoelastic fluid past a stretching surface," *Acta Mechanica*, vol. 95, no. 1-4, pp. 227–230, 1992.

[9] P. D. Ariel, "MHD flow of a viscoelastic fluid past a stretching sheet with suction," *Acta Mechanica*, vol. 105, no. 1-4, pp. 49–56, 1994.

[10] C. Y. Wang, "The three-dimensional flow due to a stretching flat surface," *Physics of Fluids*, vol. 27, no. 8, p. 1915, 1984.

[11] J. F. Brady and A. Acrivos, "Steady flow in a channel or tube with an accelerating surface velocity. An exact solution to the Navier—Stokes equations with reverse flow," *Journal of Fluid Mechanics*, vol. 112, no. 1, pp. 127–150, 1981.

[12] C. Y. Wang, "Fluid flow due to a stretching cylinder," *Physics of Fluids*, vol. 31, no. 3, pp. 466–468, 1988.

[13] C. Y. Wang, "Liquid film on an unsteady stretching surface," *Quarterly of Applied Mathematics*, vol. 48, no. 4, pp. 601–610, 1990.

[14] R. Usha and R. Sridharan, "The axisymmetric motion of a liquid film on an unsteady stretching surface," *Journal of Fluids Engineering*, vol. 117, no. 1, pp. 81–85, 1995.

[15] P. D. Ariel, "Computation of MHD flow due to moving boundary," Technical Report MCS-2004-01, Department of Mathematical Sciences: Trinity Western University, 2004.

[16] T. D. M. A. Samuel and I. M. Hall, "On the series solution to the laminar boundary layer with stationary origin on a continuous moving porous surface," *Proceedings of the Cambridge Philosophical Society*, vol. 73, no. 1, pp. 223–229, 1973.

[17] P. D. Ariel, T. Hayat, and S. Asghar, "Homotopy perturbation method and axisymmetric flow over a stretching sheet," *International Journal of Nonlinear Sciences and Numerical Simulation*, vol. 7, no. 4, pp. 399–406, 2006.

[18] M. Sheikholeslami and R. Ellahi, "Three dimensional mesoscopic simulation of magnetic field effect on natural convection of nanofluid," *International Journal of Heat and Mass Transfer*, vol. 89, pp. 799–808, 2015.

[19] W. Ibrahim and C. Zemedu, "Numerical solution of micropolar nanofluids with Soret, Dufor effects and multiple slip conditions," *Communications*, vol. 4, no. 1, article 015016, 2020.

[20] F. Javed and S. Nadeem, "Numerical solution of a Casson nanofluid flow and heat transfer analysis between concentric cylinders," *Journal of Power Technologies*, vol. 99, no. 1, pp. 25–30, 2019.

[21] R. Ellahi, S. M. Sait, N. Shehzad, and Z. Ayaz, "A hybrid investigation on numerical and analytical solutions of electromagnetohydrodynamics flow of nanofluid through porous media with entropy generation," *International Journal of Numerical Methods for Heat & Fluid Flow*, vol. 30, no. 2, pp. 834–854, 2019.

[22] M. Siavashi, H. Rasam, and A. Izadi, "Similarity solution of air and nanofluid impingement cooling of a cylindrical porous heat sink," *Journal of Thermal Analysis and Calorimetry*, vol. 135, no. 2, pp. 1399–1415, 2019.

[23] M. Subhani and S. Nadeem, "Numerical analysis of micropolar hybrid nanofluid," *Applied Nanoscience*, vol. 9, no. 4, pp. 447–459, 2019.

[24] M. A. Sadiq, A. U. Khan, S. Saleem, and S. Nadeem, "Numerical simulation of oscillatory oblique stagnation point flow of a

magneto micropolar nanofluid," *RSC Advances*, vol. 9, no. 9, pp. 4751–4764, 2019.

[25] Z. Ahmed, S. Nadeem, S. Saleem, and R. Ellahi, "Numerical study of unsteady flow and heat transfer CNT-based MHD nanofluid with variable viscosity over a permeable shrinking surface," *International Journal of Numerical Methods for Heat & Fluid Flow*, vol. 29, no. 12, pp. 4607–4623, 2019.

[26] I. Ahmad, M. A. Z. Raja, M. Bilal, and F. Ashraf, "Neural network methods to solve the Lane–Emden type equations arising in thermodynamic studies of the spherical gas cloud model," *Neural Computing and Applications*, vol. 28, no. S1, pp. 929–944, 2017.

[27] Z. Sabir, M. A. Z. Raja, M. Umar, and M. Shoaib, "Design of neuro-swarming-based heuristics to solve the third-order non-linear multi-singular Emden–Fowler equation," *The European Physical Journal Plus*, vol. 135, no. 5, pp. 1–17, 2020.

[28] Z. Sabir, H. A. Wahab, M. Umar, M. G. Sakar, and M. A. Z. Raja, "Novel design of Morlet wavelet neural network for solving second order Lane- Emden equation," *Mathematics and Computers in Simulation*, vol. 172, pp. 1–14, 2020.

[29] A. Mehmood, A. Zameer, M. S. Aslam, and M. A. Z. Raja, "Design of nature-inspired heuristic paradigm for systems in nonlinear electrical circuits," *Neural Computing and Applications*, vol. 32, no. 11, pp. 7121–7137, 2020.

[30] M. A. Z. Raja, A. Mehmood, S. A. Niazi, and S. M. Shah, "Computational intelligence methodology for the analysis of RC circuit modelled with nonlinear differential order system," *Neural Computing and Applications*, vol. 30, no. 6, pp. 1905–1924, 2018.

[31] S. I. Ahmad, F. Faisal, M. Shoaib, and M. A. Z. Raja, "A new heuristic computational solver for nonlinear singular Thomas–Fermi system using evolutionary optimized cubic splines," *The European Physical Journal Plus*, vol. 135, no. 1, pp. 1–29, 2020.

[32] Z. Sabir, M. A. Manzar, M. A. Z. Raja, M. Sheraz, and A. M. Wazwaz, "Neuro-heuristics for nonlinear singular Thomas-Fermi systems," *Applied Soft Computing*, vol. 65, pp. 152–169, 2018.

[33] M. A. Z. Raja, A. Mehmood, A. A. Khan, and A. Zameer, "Integrated intelligent computing for heat transfer and thermal radiation-based two-phase MHD nanofluid flow model," *Neural Computing and Applications*, vol. 32, no. 7, pp. 2845–2877, 2019.

[34] M. A. Z. Raja, F. H. Shah, M. Tariq, I. Ahmad, and S. . I. Ahmad, "Design of artificial neural network models optimized with sequential quadratic programming to study the dynamics of nonlinear Troesch's problem arising in plasma physics," *Neural Computing and Applications*, vol. 29, no. 6, pp. 83–109, 2018.

[35] M. A. Z. Raja, M. A. Manzar, F. H. Shah, and F. H. Shah, "Intelligent computing for Mathieu's systems for parameter excitation, vertically driven pendulum and dusty plasma models," *Applied Soft Computing*, vol. 62, pp. 359–372, 2018.

[36] I. Khan, H. Ullah, H. AlSalman et al., "Falkner–Skan equation with heat transfer: a new stochastic numerical approach," *Mathematical Problems in Engineering*, vol. 2021, Article ID 3921481, 17 pages, 2021.

[37] I. Ahmad, H. Ilyas, A. Urooj, M. S. Aslam, M. Shoaib, and M. A. Z. Raja, "Novel applications of intelligent computing paradigms for the analysis of nonlinear reactive transport model of the fluid in soft tissues and microvessels," *Neural Computing and Applications*, vol. 31, no. 12, pp. 9041–9059, 2019.

[38] S. Akbar, M. A. Z. Raja, F. Zaman, T. Mehmood, and M. A. R. Khan, "Design of bio-inspired heuristic techniques hybridized with sequential quadratic programming for joint parameters estimation of electromagnetic plane waves," *Wireless Personal Communications*, vol. 96, no. 1, pp. 1475–1494, 2017.

[39] J. A. Khan, M. A. Z. Raja, M. M. Rashidi, M. I. Syam, and A. M. Wazwaz, "Nature-inspired computing approach for solving non-linear singular Emden–Fowler problem arising in electromagnetic theory," *Connection Science*, vol. 27, no. 4, pp. 377–396, 2015.

[40] M. A. Z. Raja, T. Ahmed, and S. M. Shah, "Intelligent computing strategy to analyze the dynamics of convective heat transfer in MHD slip flow over stretching surface involving carbon nanotubes," *Journal of the Taiwan Institute of Chemical Engineers*, vol. 80, pp. 935–953, 2017.

[41] M. A. Zahoor Raja, Z. Shah, M. Anwaar Manzar, I. Ahmad, M. Awais, and D. Baleanu, "A new stochastic computing paradigm for nonlinear Painlevé II systems in applications of random matrix theory," *The European physical journal plus*, vol. 133, no. 7, p. 254, 2018.

[42] S. Lodhi, M. A. Manzar, and M. A. Z. Raja, "Fractional neural network models for nonlinear Riccati systems," *Neural Computing and Applications*, vol. 31, no. S1, pp. 359–378, 2019.

[43] I. Khan, H. Ullah, M. Fiza et al., "A Levenberg-Marquardt backpropagation method for unsteady squeezing flow of heat and mass transfer behaviour between parallel plates," *Advances in Mechanical Engineering*, vol. 13, no. 10, pp. 1–15, 2021.

[44] M. Fathizadeh, M. Madani, K. Yasir, F. Naeem, Y. Ahmet, and T. Serap, "An effective modification of the homotopy perturbation method for MHD viscous flow over a stretching sheet," *Journal of King Saud University-Science*, vol. 25, no. 2, pp. 107–113, 2013.

[45] Podlubny, *Fractional Differential Equations*, Academic press, New York, 1999.

[46] M. Caputo, *Elasticita e Dissipazione*, zani-Chelli, Bologna, 1969.